ORIGINAL ARTICLE
DOI: https://doi.org/10.18599/grs.2024.4.20

Advanced Well Logging Interpretation for Reliable Electrotyping of Low-permeable and Low-resistivity Formation

A. Thistiakov[1], E. Shvalyuk[1], K. Okosun [1], M. Spasennykh[1], A. Stenin[2]*
[1]*Skolkovo Institute of Science and Technology, Moscow, Russian Federation*
[2]*LUKOIL Engineering LLC, Moscow, Russian Federation*

Abstract. The target formation of a brown oilfield in Western Siberia is composed of a shallowing-up succession represented by siltstones in its base gradually replaced by sandstones toward its top. Due to the absence of detailed rock- and electrotyping, the siltstones, having much lower resistivity and permeability, were assigned to a water-bearing section. However, the following up well tests detected considerable oil inflow from them as well. This motivated current research aimed at developing a new methodology of rock- and electrotyping of low-resistive, low-permeable clastic reservoirs. The methodology comprises detailed workflow for laboratory tests, rock typing by means of the alternative flow zone indicator (*FZI*), and, finally, transfer of core-derived rock types to well log electrotypes. The proposed application of the dimensionless *FZI* parameter, incorporating porosity and irreducible water saturation, appeared to be very effective for electrotyping of the formation, including low-resistive and low-permeable intervals.

Since the intervals are characterized by a low correlation between permeability and porosity, applying the latter log for computing permeability results in unreliable calculation of the parameter and further incorrect electrotyping. In order to resolve this issue, the study suggests an effective alternative technique for calculating permeability as a multivariate parameter from other logs.

Further, the research proposes a well log interpretation workflow that enables conversion of the defined rock types to electrotypes, maintaining the same classification principles for both core and well logs data. This ensures compatibility of the core and well log-derived classes.

The petrophysical interpretation workflow is enhanced with machine learning algorithms for reconstructing lacking logs as well as extending the defined electrotypes to uninterpreted wells. The proposed approaches to rock- and electrotyping allows detection of previously missed productive intervals and thus enables extend the lifetime of the brownfield.

Keywords: well logging; rock typing; low-resistivity reservoirs; electrotyping; machine learning

Recommended citation: Thistiakov A., Shvalyuk E., Okosun K., Spasennykh M., Stenin A. (2024). Advanced Well Logging Interpretation for Reliable Electrotyping of Low-permeable and Low-resistivity Formation. *Georesursy = Georesources*, 26(4), pp. 163–175. https://doi.org/10.18599/grs.2024.4.20

1. Introduction

The prime objective of rock typing is dividing rock samples into clusters that can be characterized by a common set of equations describing relationships between the key rock parameters used for reserves and production rate calculation (Gholami et al., 2009; Shvalyuk et al., 2021). Electrotyping is aimed at deriving from well logs of formation intervals, corresponding to the rock types established for the core (Curtis et al., 2015).

It is worth mentioning that rock and electrotyping are commonly based on survey of different rock volume and measured characteristics. Moreover, translation of core rock types to electrotypes lacks unified approaches, and is often disputable, particularly, when limited well logging and core data are available (Guo et al., 2007; Aranibar et al., 2013; Gupta 2017; Perry et al., 2019).

The most popular rock and electrotyping procedures involve differentiation on porosity-permeability. For example, rock typing, based on defining "Flow Units" (Amaefule et al., 1993; Tiab et al., 2016), includes calculation of two classification parameters, namely flow zone indicator (*FZI*) and reservoir quality index (*RQI*) (Abbaszadeh et al., 1996; Teh et al., 2012; Kassem et al., 2017). *FZI* is commonly calculated as a function of porosity and permeability. If we apply core data for *FZI* calculation, these two parameters are measured with different tests independently of each other. At the same time, if *FZI* is derived from well logs, the applied permeability is calculated from the porosity log by means of correlation equations. Thereby, the process of electrotyping loops on differentiation mainly by log-derived porosity values.

Other commonly used concepts for rock typing and consequent permeability calculation, such as Winland or

*Corresponding authors: Alexei Tchistiakov
e-mail: A.Tchistiakov@skoltech.ru

Pittman (Kolodzie, 1980; Pittman, 1992), link porosity, permeability, and representative pore throat radius, corresponding to a certain mercury saturation during a MICP test. At least two arguments can be opposed to these concepts. First, fluid flow is controlled by more than one pore throat radius size, thus the representativeness of the applied singe value is disputable (Mirzaei-Paiaman et al., 2018). Second, these concepts remain dependant on primarily linking porosity with permeability, as in the "Flow Units" theory. Thus, in order to ensure involvement of permeability as independent variable in rock typing, it must be calculated from well logs other than porosity.

Permeability is controlled by multiple bulk and microstructural rock characteristics, such as porosity, irreducible water saturation, pore size distribution, tortuosity, connectivity, rock mineralogy, wettability and others (Mustafa et al., 2019; Saxena et al., 2019; Eltom, 2020). Due to this fact, representative calculation of permeability should be based on well logs influenced by similar factors. Because electrical current conductivity and ion diffusion are subjected to equivalent rock's microstructural characteristics as fluid filtration, resistivity as well as spontaneous potential (SP) logs can potentially be used for permeability assessment, (Pirson et al., 1963; Smits, 1968; Coates, Dumanoir 1973; Abbaszadeh et al., 1996; Ma et al., 2015).

Unfortunately, many fields suffer from inconsistency or lack of core and well logging data that reduces the reliability of rock and electrotyping. This, in turn, results in missing producing intervals and miscalculating hydrocarbon reserves. This poses a need for advanced approaches to data reconstruction, including machine learning algorithms. Moreover, applying sophisticated machine learning algorithms for extension of electrotypes, defined by a petrophysicist, to wells, where neither core nor well log interpretation was done, will increase the reliability of the reservoir delineation, particularly in disputable zones, where applying conventional simplistic threshold-based models can produce bias results (Akkurt et al., 2018; Perez et al., 2005; Man et al., 2021; Merembayev et al., 2021).

The target formation of a brown oilfield in the Western Siberia is composed of a shallowing up succession, represented by siltstones in its base, gradually replaced by sandstones toward its top. The siltstones are characterized by low electrical resistivity and permeability, and thus were previously assigned to a water-bearing part of the reservoir and excluded from the production. However further well tests showed oil inflow from them as well. Therefore, development of new alternative petrophysical interpretation methodology for the formation was needed in order to correctly reassess its production potential.

Considering the low-permeable and low-resistive formation characterization issues mentioned above, the main objective of this work is to provide a new advanced petrophysical interpretation, enabling reliable identifying electrotypes using core and conventional well logging data.

This requires accomplishing the following tasks:

• Proposing an alternative rock typing index, acknowledging the microstructural characteristics of the low-resistive formation.

• Developing an alternative permeability calculation technique, not engaging porosity logs, in order to ensure independence of all entities in the applied rock typing index.

• Conversion of defined rock types to electrotypes, maintaining the same classification principles for both core and well logs data.

• Implementation of machine learning for logs reconstruction and automatic extension of defined electrotypes to manually uninterpreted wells.

2. Materials and Methods

2.1. Core and Well-logging Data Interpretation

An overall workflow applied in the research for electrotyping is shown in Figure 1.

The results of routine core analyses (RCAL) and special core analyses (SCAL), comprises:

• Helium porosity (φ) and permeability with the Klinkenberg correction (k);

• Rock bulk (ρ_b) and grain (ρ_{ma}) densities;

• Capillary pressure curves obtained in "gas-water" system and residual water saturation (S_{wir});

• Resistivity measurements;

• Nuclear magnetic resonance (NMR) spectra, obtained before centrifuging (S_w = 100%) and after centrifuging ($S_w = S_{wir}$);

• Computed tomography (CT) scanning;

• X-ray diffraction (XRD);

Well logging data includes:

• Gamma ray (12 wells);

• Spontaneous Potential (12 wells);

• Neutron log (12 wells);

• Resistivity log (12 wells);

• Density log (7 wells);

• Sonic log (12 wells, including 6 with recorded logs and 6 with reconstructed one by means of ML).

Well logging data interpretation includes a preliminary synthesis of absent well logs by means of multilinear regressions (MLR). Afterwards, lithotyping, mineralogical composition φ, k, S_{wir} and FZI are calculated. The mineralogical model and well log-derived φ are calibrated on core XRD and porosity data. Permeability is calculated with multilinear regression as a function of clay volume (V_{clay}), normalized micro-resistivity (R_{norm}) and relative parameter of spontaneous potential log (ASP).

Equation for R_{norm} calculation is:

$$R_{norm} = \frac{log\, R_{XO}^{max} - log\, R_{XO}}{log\, R_{XO}^{max} - log\, R_{mud}} \quad (1)$$

where R_{norm} is normalized resistivity, R^{XO} is flushed zone resistivity, $R_{XO}{}^{max}$ is the resistivity value in a thick dense layer, R_{mud} is drilling mud resistivity. The micro-resistivity, measured within the flushed zone, is applied to exclude the influence of formation fluid, which can vary with depth.

ASP parameter is calculated as follows:

$$ASP = \frac{PSP - SSP}{SP_{clay} - SSP} \quad (2)$$

where PSP is pseudo-static spontaneous potential, which is the SP deflection obtained for clay beds, SSP is a static spontaneous potential of a nearby thick, clean sand (Glover, 2000).

S_{wir} is derived from the correlation between φ and k, obtained for core data.

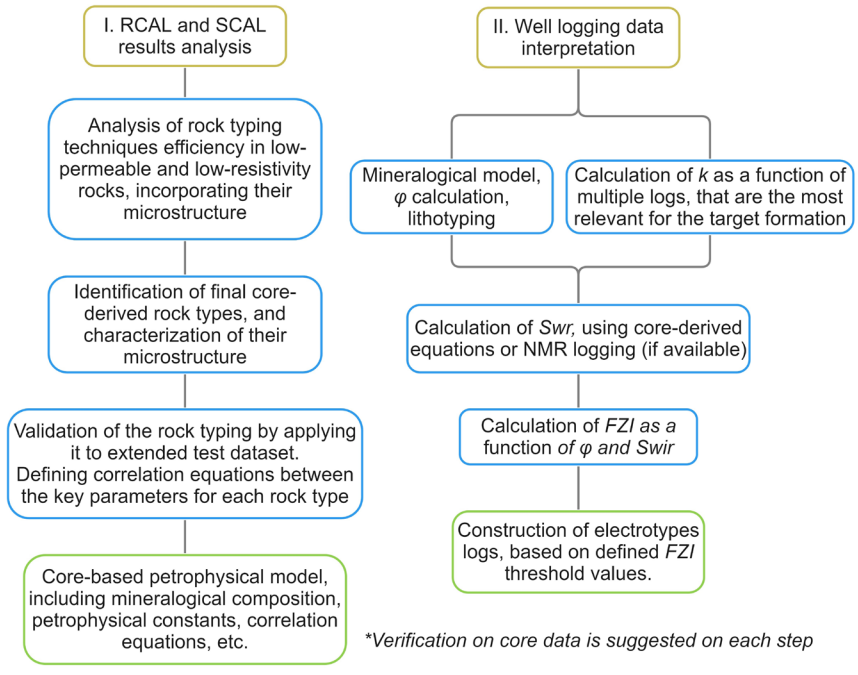

Figure 1. Methodology for reliable rock typing of low-resistive and low-permeable formations based on core and well logging data interpretation

Flow Zone Indicator (*FZI*) is calculated from the reservoir quality index (*RQI*) and φ as follows (Amaefule et al., 2006; Tiab et al., 2016):

$$RQI = 3.14 \cdot \frac{\varphi \cdot (1-S_{wir})}{\varphi - \varphi \cdot (1-S_{wir})} \cdot \sqrt{\varphi^3} \quad (3)$$

$$FZI = RQI \cdot \frac{1-\varphi}{\varphi} \quad (4)$$

While the conventional *RQI* and *FZI* are calculated as a function of porosity and permeability, we apply a dimensionless *FZI* parameter derived from porosity and irreducible water saturation. This approach is appeared to be more appropriate for the low-permeable rocks typing, because they vary to a greater extent in irreducible water saturation rather than in permeability values, which are close to the lower threshold of instrumental measurement.

3. Results

3.1. Core Rock Types Identification

Rock typing is done based on integrated interpretation of flow zone indicator (*FZI*) with the results of porosity-permeability measurements, centrifuging, resistivity, NMR and CT-scanning tests. Analysis of the cumulative curve of *FZI* and the porosity versus permeability plot, shown in Figure 2,

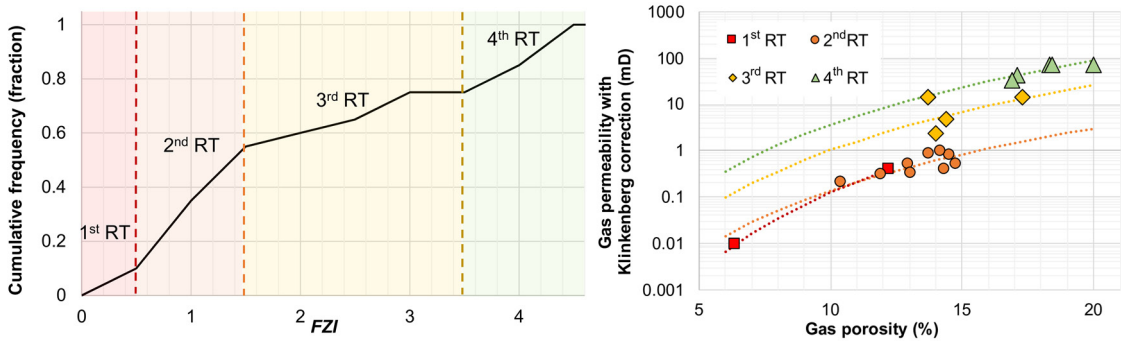

Figure 2. a) cumulative curve of FZI values for RTs Identification and b) porosity versus permeability plot for four RTs identified by means of integrated interpretation of FZI, RCAL and SCAL results

RT	*FZI*	S_{wir} (%)	Grains diameters (mm)	M_e (μm)	M_o (μm)	Pores with radius less than 0.32 μm (%)	Group $T_{2cutoff}$ (ms)	Saturation exponent *n*	Cation exchange capacity, (eq/L)
1st	<0.5	>79.09	<0.005	<0.032	<0.032	64–70	5–6	0.92	0.188
2nd	0.5–1.5	45.2–60.3	0.02–0.12	0.032–0.08	0.032–0.6	37–52	5–6	1.45	0.112
3rd	1.5–3.5	26.43–32.52	0.1–0.25	0.2–0.7	0.6–5.6	18–30	11–12	1.91	0.062
4th	>3.5	<22.44	0.2-0.4	1.1–1.4	3.2–10	13–17	11–12	2.1	0.056

Table 1. Summary table of rock types quantitative characteristics. FZI is flow zone indicator, S_{wir} is irreducible water saturation, M_o and M_e are ranges of modal and median pore radii, $T_{2cutoff}$ is a transverse relaxation time of the cut-off value

allows confident distinguishing of 4 rock types (Table 1). The characteristic results of CT-scanning, NMR studies and capillary pressure tests for each individual rock type (RT) are presented in Figure 3 and Figure 4.

The 1st RT is composed of tight, fine-grained, low-permeable siltstones with massive microstructure lacking a visible connected system of pores. The connectivity of the porous network can be affected by different factors, such as carbonate cementation or poor grains' sorting. Pores with a radius less than 0.032 μm prevail. $T_{2cutoff}$ for this RT is the lowest and its spectra at irreducible and full water saturations are close to each other, which indicates that almost all porous space is filled with irreducible water (Figure 3 and Figure 4).

The 2nd RT comprises siltstone and tight sandstone samples with porosity ranging from 10–15% and permeability less than 1 mD. The porous media of this RT mainly consists of tiny not well-connected pores with radii varying from 0.032 to 0.56 μm. The grain size of the RT varies from 0.02 to 0.12 mm. Several samples contain carbonate grains and clay seams, which are clearly observed as light inclusions and lines in the CT-scan images. The samples of the 2nd rock, similarly to the 1st one, are characterized by low $T_{2cutoff}$ values. Nevertheless, the proportion of interconnected effective porosity, according to NMR spectra and CT-scans, is higher in the 2nd RT (Figure 4).

The 3nd RT is represented by silty sandstones. The sand grains from 0.1 to 0.25 mm in diameter dominate, although the total grain size distribution is in the range from 0.05 to 0.4 mm. The permeability values reach 15 mD. The pores radii are presented mostly in range from 0.6 to 5.6 μm. The space available for free fluids filtration is much larger as compared

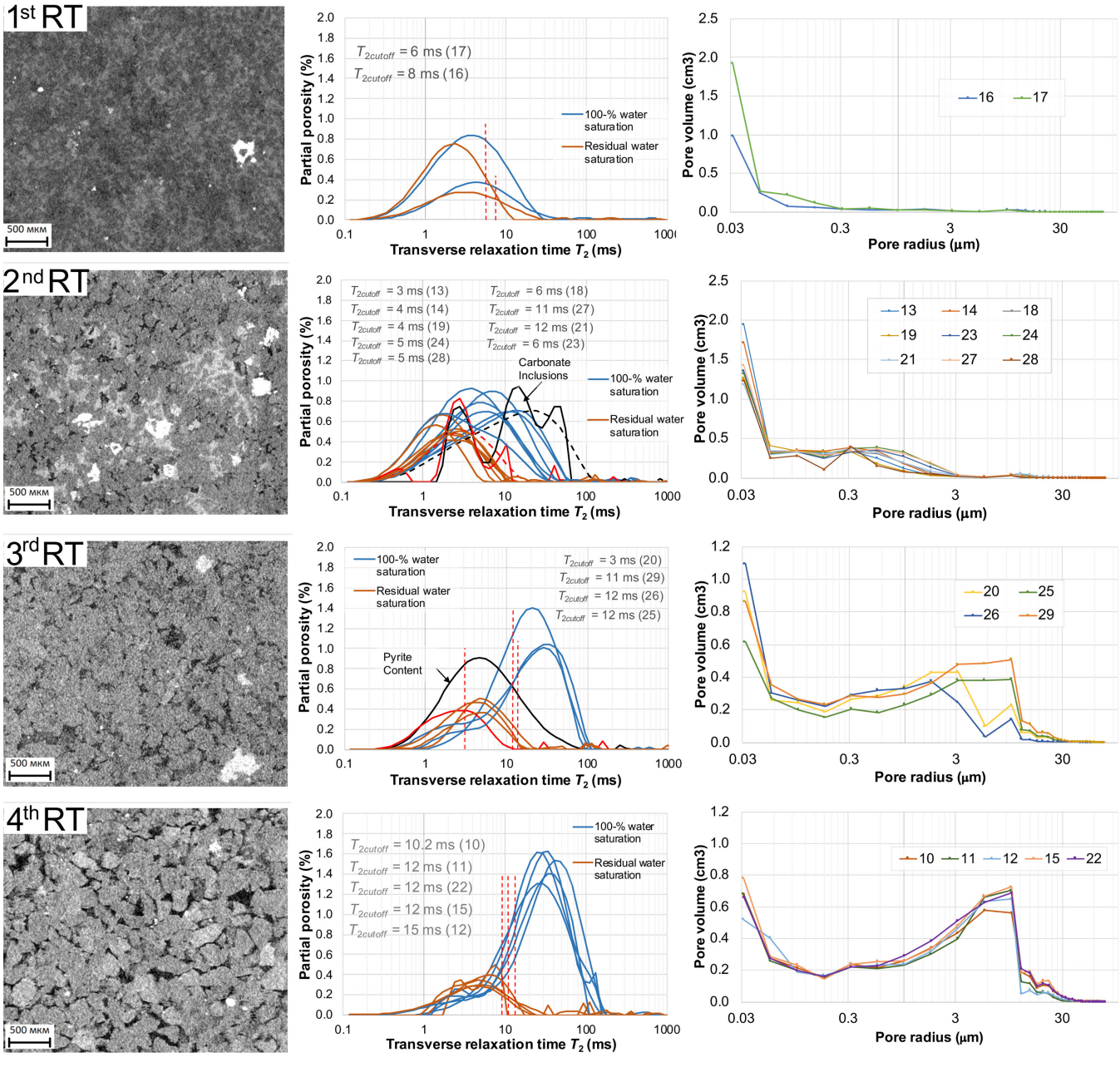

Figure 3. The characteristic results of CT-scanning, NMR studies and capillary pressure tests regarding established rock types (from the left to the right): 1) 2D CT-scans: brighter pixels have high absorption and represent a denser phase of the mineral matrix of the rock. In the studied rock, pyrite has the highest X-ray adsorption capacity, calcite has medium value, and quartz, feldspars – the lowest; 2) NMR spectra and identified $T_{2cutoff}$ values (the samples' numbers are shown in brackets); 3) pore radii distributions, combined from CT and capillary pressure tests results

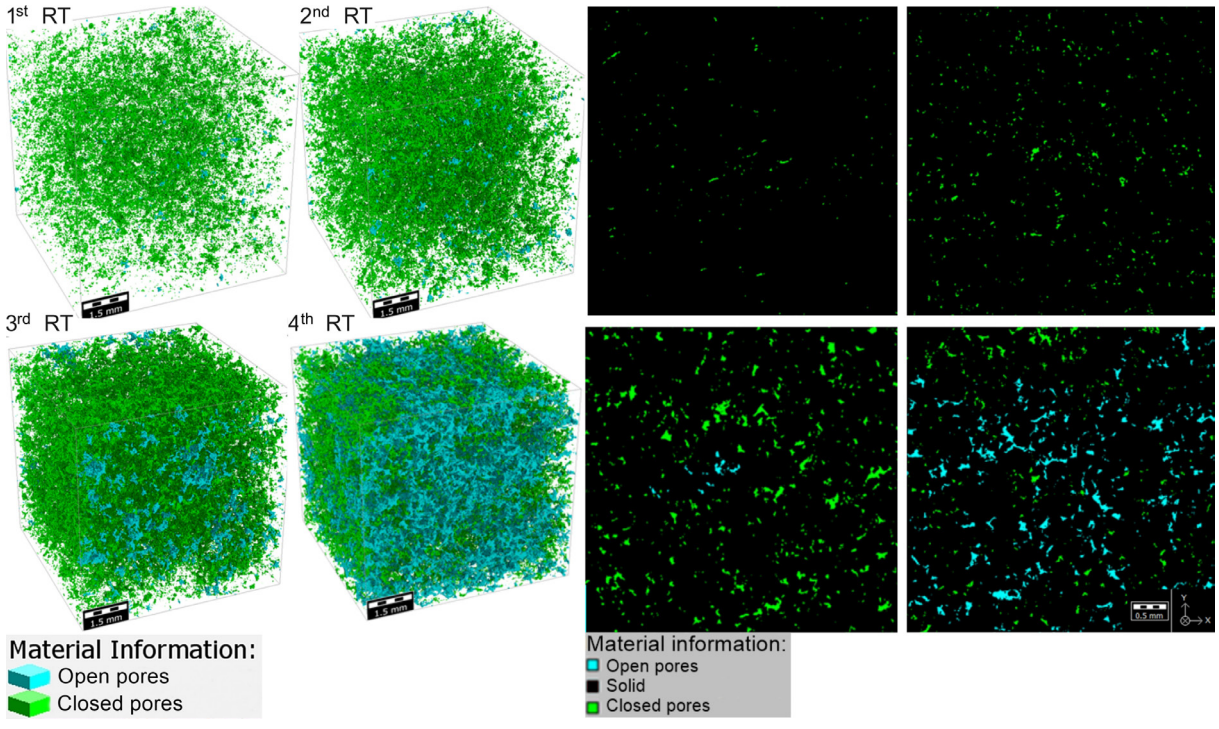

Figure 4. 3D distributions of open (blue colour) and closed (green colour) pores by means of CT-scanning

with the 2nd and 3nd RTs, and the fraction of irreducible water is less than 33% (Table 1).

In the sandstones of the 4th RT the grains with a diameter of 0.2–0.4 mm dominate, while the total grain size distribution extends from 0.05 to 0.6 mm (Figure 4). Permeability is relatively high, ranging from 30 to 74 mD. The RT is characterized by a well-developed network of large pores, varying in radii from 3.2 μm to 10 μm. According to NMR spectra and capillary pressure tests this rock type has the least irreducible water saturation (S_{wir} < 23%) (Figure 3 and Figure 4). Thus, the 4th RT composes the best part of the reservoir.

The saturation exponent n consistently decreases from the 4th to the 1st RT. This trend corresponds to mineral fraction fining and the consequent increase in irreducible water content, resulting in higher conductivity. The increase of the fine fractions from the 1st to the 4th RT is also reflected in the growth of the volumetric cation exchange capacity (CEC), characterising the specific surface of the rocks (Table 1).

The rock typing, derived from joint interpretation of SCAL and RCAL tests for a limited set of 20 samples, is extended to a data set for 700 samples. The increase of the data set does not change the *FZI* border between the 1st and 2nd RTs. However, the boundary between 3nd and 4th RTs is shifted from 3.5 to 2 (Figure 5). Thus, it can be concluded that the applied rock typing approach shows good sustainability to significant increase of the quantity of data.

3.2. Integrated Well Log Interpretation

The well log interpretation yields the following logs: lithological and mineralogical composition, porosity, permeability, irreducible water saturation, and electrotypes. The layouts for 2 representative wells are shown in Figure 7, and Figure 8. The formation comprises five main lithotypes, including sandstones, siltstones, claystones, coals and

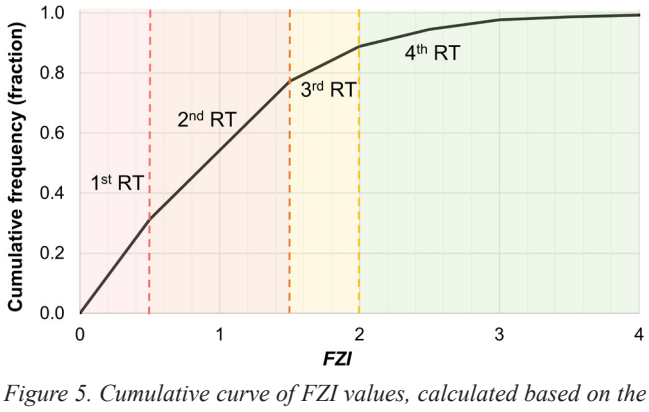

Figure 5. Cumulative curve of FZI values, calculated based on the extended core analyses results

dense rocks (practically impermeable). The mineralogy is represented by quartz, feldspar, clay minerals and carbonate inclusions. The log-derived mineralogy is calibrated on XRD data.

For permeability calculation we investigate the possibilities to use its correlation with single logs, namely clay volume content (V_{clay}), spontaneous potential (*ASP*), normalized micro-resistivity (R_{norm}), as well as multiple correlation with all these logs.

Clay volume (V_{clay}) usually correlates with residual water content, controlling effective porosity. This explains previous attempts of other authors to use this log for permeability calculation of clastic reservoirs (Nelson, 1994; Vernik, 2000). However, in our formation bound water is considerably associated with silt fraction. Thus, applying a single correlation between V_{clay} and permeability does not enable its sufficient match with the one measured on core. The correlation coefficient (R) in the equation, relating core-derived *k* and well-derived V_{clay}, amounts to just 0.53.

The SP amplitude is influenced by both clay volume and porosity (Smits, 1968). As the result, in the considered formation permeability appears to have higher correlation with *ASP* (R = 0.78) than with V_{clay}. However, because SP log has relatively low spatial resolution, for permeability calculation it should be accompanied by other logs.

While V_{clay} and *ASP* represent mainly bulk properties of the rock, electrical resistivity responds much stronger to porous network characteristics, such as size distribution, tortuosity, connectivity and so on. This explains the observed strongest correlation (R = 0.85) between permeability and resistivity logs.

Permeability, derived from the multiple logs (R_{norm}, V_{clay} and *ASP*) is appeared to have the best correlation (R = 0.87) with core-measured permeability. For comparison, the coefficient of correlation between permeability and total porosity log amounts only R = 0.56.

Following the permeability prediction, the irreducible water was also calculated from borehole logs. Since independent well logging data on S_{wir}, such as NMR logging, was not available, S_{wir} was calculated based on the correlation function of porosity and permeability, measured on core (equation 5):

$$S_{wir} = 0.79\sqrt{\frac{k}{\varphi}}^{-0.17}, R=0.91 \quad (5)$$

3.3. Electrotyping

FZI is calculated with equations (3) and (4). The *FZI* boundary values, derived from core and log data, are equal to each other (Figure 5 and Figure 6). This enables consistent transfer of core-derived types to electrotypes, shown together with the lithology log and core data Figure 7 and Figure 8. Average properties and mineralogical composition for each electrotype are presented in Table 2.

The 1st electrotype is represented mainly by siltstones (60 %) and claystones (24%), it also includes some 14% of dense rocks and 2% of coals.

The 2nd electrotype is composed of siltstones (54%), claystones (23%), sandstones (19%), and dense rocks (some 4%). The 3rd and 4th electrotypes are represented mainly by sandstones, 76% and 96%, respectively.

The 4th electrotype is characterized by the highest φ and k, as well as by the lowest S_{wir}, and is considered the "best reservoir".

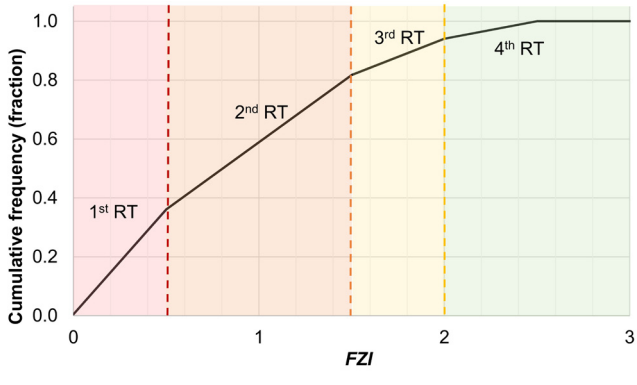

Figure 6. Cumulative curve of FZI values, calculated from well logs interpretation

3.4. Application of Machine Learning for Well Log Reconstruction and Electrotyping

Machine learning (ML) in this research was used for i) reconstruction of sonic logs, absent in a number of wells and ii) automatization of petrophysical interpretation of logs in remaining wells of the field. First, we describe well logs reconstruction, then we discuss the selected algorithms for electrotyping, and finally we present the results of ML-based interpretation (Figure 9).

3.4.1. Well Logging Data Reconstruction using MLR

Wells at the target field often lack density and sonic logs, those are essential for petrophysical interpretation, including construction of a mineralogical model. Thus, this study attempts to synthesize them by applying multilinear regressions. It appears that confidence of density log reconstruction is relatively low. Its influence on electrotype prognosis with ML is also insignificant.

Reconstruction of sonic logs (DTP) on the contrary produces reliable result (Figure 10). The compressional slowness, measured in sonic logging, depends mainly on rock bulk density, mineralogical composition and fluid saturation. Therefore, gamma ray (GR), neutron (NPOR) and recorded density logs are selected as the most relevant entities for sonic log generation. If a density log is not present, only NPOR and GR logs are applied. The corresponding correlation equations are shown below:

DTP_REC = –87.88·DENSITY + 373.2·NPOR + 0.005·GR + 404.87, R = 0.82, RMSE = 32.33" (6)

DTP_REC_2 = –0.01·GR + 480.52·NPOR + 170.04, R = 0.8, RMSE = 34.132" (7)

The comparison of the reconstructed sonic logs (DTP_REC and DTP_REC_2), calculated from these two equations, with a reference sonic log (Figure 10) confirms the high reliability of ML applied for the log reconstruction.

3.4.2. ML Algorithms Applied for Electrotyping

The ML workflow, used in this research, includes data gathering and integration, feature ranking/selection, standardization, cross-validation, model development, grid search for parameter fine tuning and optimization, and trained model implementation. Feature selection and ranking are performed by using data visualization utilities such as the Pearson correlation coefficient and ranking importance plots. The well data is split into training and test sets consisting of five training wells, selected based on their data quality.

In order to select the most efficient method, three supervised ML algorithms, namely the support vector machine (SVM), extreme gradient boost (XGB) and multi-layer perceptron (MLP) are applied. The input data set for prediction includes DTP, GR, R_{norm}, NPOR, density and *ASP*.

Support vector machine is a supervised machine learning algorithm that can be used to solve classification and regression problems. Particularly, it is applied for various geoengineering purposes, including electrofacies classification and lithology interpretation. Those tasks are based on similar principles as electrotypes identification regarding prediction of specific intervals using well logs and reference flag-curves of any geological classes. SVM's operate on the concept of a "margin", which is either side of a hyperplane, that separates two data classes (Cortes, Vapnik, 1995).

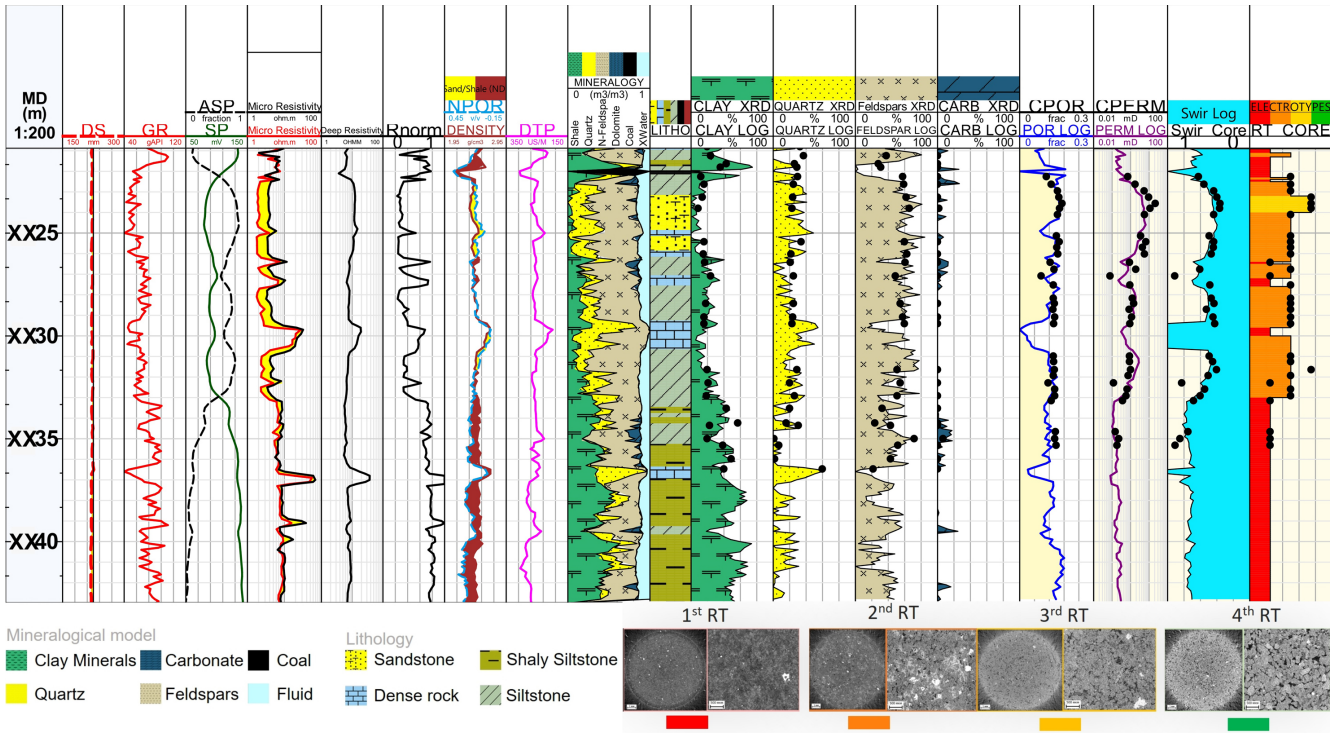

Figure 7. Layout for one of the well: 1st track – measured depth (MD) (m); 2ndtrack – calliper (DS) (mm); 3nd – gamma ray log (GR) (API); 4th track – spontaneous potential log (SP) (mV) and relative SP parameter (ASP) (v/v); 5th track – micro-potential and micro-gradient resistivity logs (Ohm·m); 6th track – deep resistivity log (Ohm·m); 7th track – normalized micro-resistivity; 8th track – neutron (NPOR) (v/v) and density (g/cm³) logs; 9th track – compressional slowness (DTP) (μs/m); 10th track – mineralogical model (v/v); 11th track – lithological column; 12-15th tracks – clay minerals, quartz, feldspars and carbonate contents (%) with core data points from XRD; 16th track – log- (POR_LOG) and core-derived (CPOR) total porosity (v/v); 17th track – log- (PERM_LOG) and core-derived (CPERM) permeability (mD); 18h track – log- (S_{wir}_Log) and core-derived (S_{wir}_Core) irreducible water saturation (v/v); 19th track – log- and core-derived rock- and electrotypes

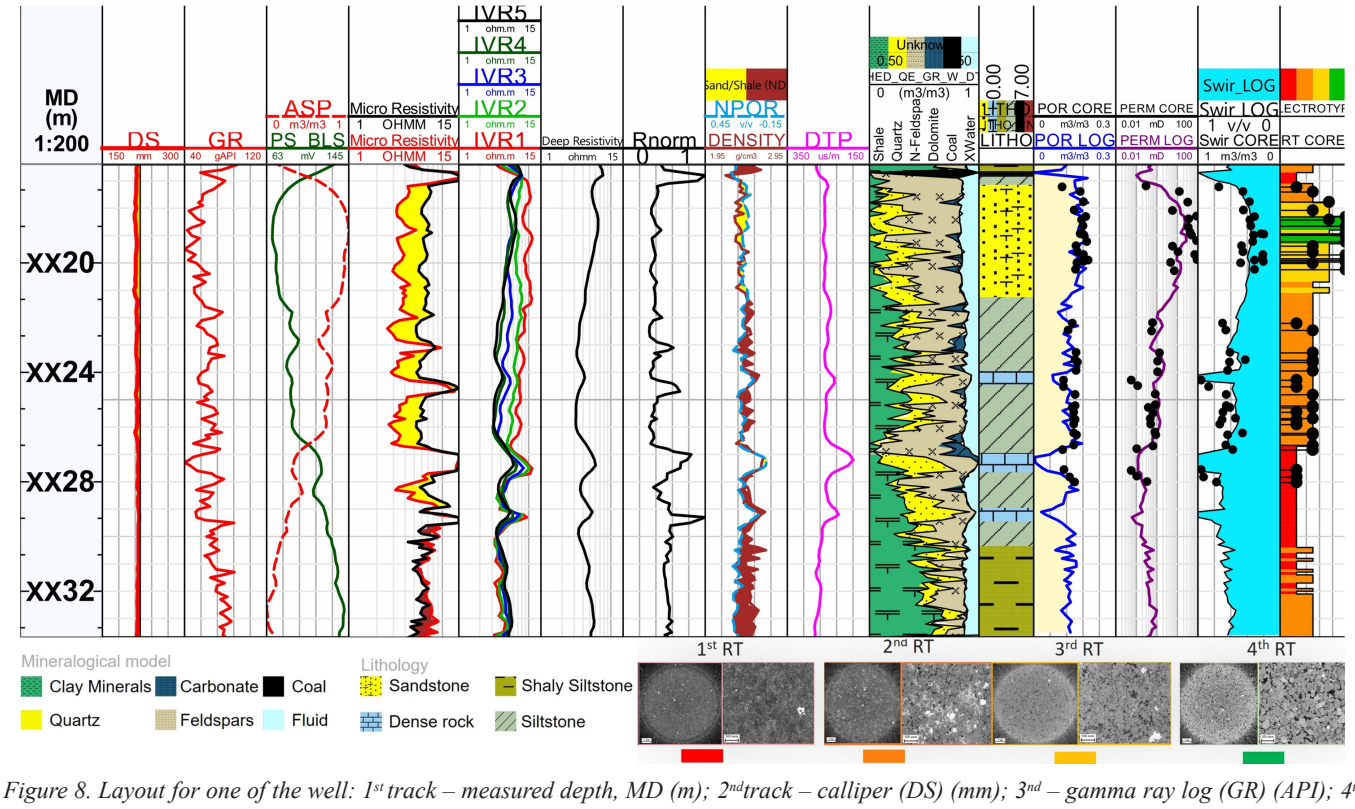

Figure 8. Layout for one of the well: 1st track – measured depth, MD (m); 2ndtrack – calliper (DS) (mm); 3nd – gamma ray log (GR) (API); 4th track – spontaneous potential log (SP) (mV) and relative SP parameter (ASP) (v/v); 5th track – micro-potential and micro-gradient resistivity logs (Ohm·m); 6th track – high frequency isoperimetric induction logging (Ohm·m); 7th track – deep resistivity log (Ohm·m); 8th track – normalized resistivity; 9th track – neutron (NPOR) (v/v) and density (g/cm³) logs; 10th track – compressional slowness (DTP) (μs/m); 11th track – mineralogical model (v/v); 12th track – lithological column; 13th track – log- (POR_LOG) and core-derived (CPOR) total porosity (v/v); 14th track – log- (PERM_LOG) and core-derived (CPERM) permeability (mD); 15th track – log- (S_{wir}_Log) and core-derived (S_{wir}_Core) irreducible water saturation (v/v); 16th track – log- and core-derived rock- and electrotypes

Electrotype	*FZI*	S_{wir} (%)	φ (%)	*k* (mD)	Quartz (%)	Feldspar (%)	Clay minerals (%)	Carbonate (%)
1st	<0.5	64.1	10.4	0.3	8.9	42.4	32.8	1.5
2nd	0.5–1.5	55.0	11.1	0.9	11.7	39.0	36.0	2.0
3rd	1.5–2	36.9	14.6	12.7	20.1	53.5	7.8	8.2
4th	>2	33.4	16.4	25.8	19.9	58.8	1.8	2.9

Table 2. Summary table of electrotypes quantitative characteristics. FZI is a flow zone indicator; S_{wir} is an average irreducible water saturation; k is a geometric mean value of permeability

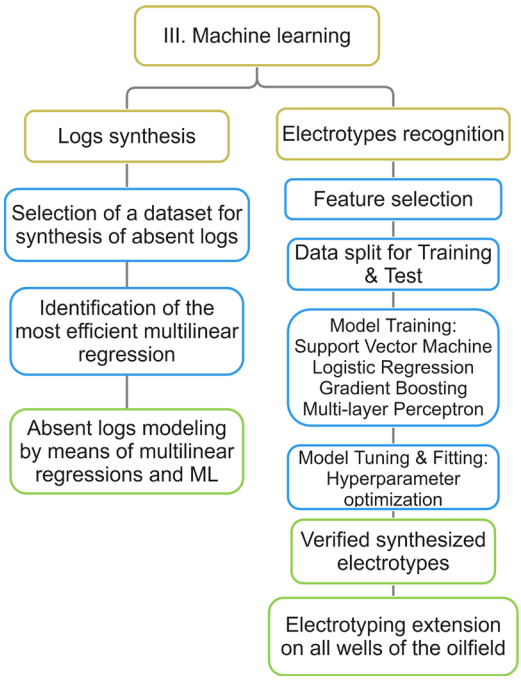

Figure 9. Application of ML for well log reconstruction and electrotyping

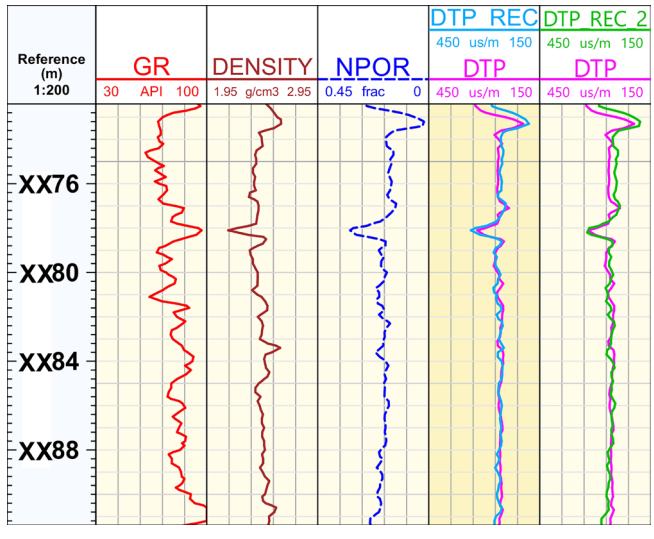

Figure 10. An example of sonic log synthesis using MLR; measured sonic log (pink) and reconstructed (DTP_REC is calculated from GR, density and NPOR; DTP_REC_2 is calculated from GR and W)

Let's consider a labelled dataset consisting of N pairs (x_i, y_i), where x_i is the i^{th} feature vector, and y_i is the i^{th} class label. Assume, that there are two classes, and that y_i is either 1 or −1. It is possible to predict the sign of y for any point x using a linear classifier, so that for a new x, we can predict $\hat{y}$ by means of equation (8):

$$\hat{y} = sign(a^T x + b) \quad (8)$$

In this equation a and b represent a hyperplane, given by the points $a^T x+b=0$. Notice, that the magnitude of $a^T x+b$ grows as the point x moves farther away from the hyperplane. Maximizing the margin and, as a result, establishing the greatest possible distance between the separating hyperplane and the instances on either side of it has been shown to lower the upper bound on the expected generalization error (Kotsiantis, 2007). This hyperplane separates the positive data from the negative data and is an example of a decision boundary. When a point crosses the decision boundary, the predicted label for that point changes (Sarkar et al., 2018).

Boosting is an ensemble modeling technique that attempts to build a strong classifier from the number of weak classifiers. This is achieved by adding new weak models to the ensemble sequentially. First a base model is built from the training data. Thereafter, on each iteration, a newer model is introduced into the bloc which tries to correct errors of the previous models:

$$y_{true} = \alpha_1 M_1(\vec{x}) + \gamma_1 \quad (9)$$

where α_1 denotes the corresponding weight for the first weak model $M_1(\vec{x})$.

Sequential model training uses gradient boosting, to gradually minimize a loss function. Based on this concept, the predicted output becomes equal to the predictions of all weak models, as shown in equation (10):

$$y_{pred} = \sum_{i=1}^{N} \alpha_i M_i(\vec{x}) \quad (10)$$

where N denotes the number of weak models. The loss function is minimized in the same manner as an artificial neural network model in which weights are optimized. Following the constructing of the weak learners in gradient boosting, the predictions are compared with the actual values using the equation:

$$\varepsilon_l = \frac{1}{2}\left|y_{pred} - y_{true}\right|^2 \quad (11)$$

The difference between prediction and actual values represents the model error rate. It can be used to calculate the gradient, which is essentially the partial derivative of the loss function. The gradient is used to determine the direction in which model parameters must be modified to reduce error in the subsequent training phase. Compared with neural network models, where the main function is to minimize a loss function in a single model, gradient boosting combines the predictions of numerous models. The gradient boosting algorithm is usually applied for lithology prediction.

The ***MLP*** algorithm uses a multi-layer neural network. It is constructed of a large number of units (neurons), which are connected in a pattern. In a network, units are typically classified into three types: input units, which receive

information for processing; output units, which contain the results of the processing; and hidden units, which are located in the middle. The hidden unit, containing one or more non-linear units, distinguishes it from other algorithms. The connection between each pair of nodes is represented by weights, w_{ij}, in which i and j represent nodes in the input and output layers, respectively. The weight, as a given value, is comparable with the electrochemical signal's strength. Computations on the input units (I_i) in the hidden layer(s) (h_j) are performed by using weights and biases:

$$h_j = \sum_{i=1}^{N} w_{ij} \cdot I_i + \theta_j \quad (12)$$

In the equation the bias θ_j is a pseudo node, having an output value of 1 that is applied, when the input value is 0. As the final step for each node h_j output value is computed using an activation function (F) that determines the signal amplitude based on the action potential of the node:

$$\theta j = F(h_j) \quad (13)$$

The MLP algorithm is applied mainly for electrofacies classification and lithology interpretation, as well as for prediction of petrophysical properties of rock sequences in non-cored wells, hydraulic flow unit classification and prediction.

To sum up, the ML classification algorithms operate based on different mathematical principles. As a result, they produce unidentical results. Therefore, to establish the most appropriate algorithm for electrotyping, the comparison of their performance should be done. Performance metrics, such as accuracy, precision, recall, F1-score, as well as support and confusion matrices are used to assess the model's predictive quality. The stratified k-fold cross-validation procedure is applied for estimation of the algorithm's performance on unseen data. This technique usually results in a less biased or less optimistic estimate of the model's opportunities than other methods.

3.5. ML Results of ML-based Electrotyping

The comparison of electrotypes distribution predicted by ML and interpreted by a petrophysicist is shown in Figure 11. The mean accuracy for each algorithm is obtained with the stratified k-fold cross-validation technique on the available dataset. A k-fold of 10 is used for the electrotype samples. The MLP algorithm appears to provide the best scoring results for the prediction of electrotypes (Table 4).

Table 3 presents a summary of the performance metrics for electrotypes, predicted by ML, against electrotypes, derived from well logs interpretation. The electrotypes predicted by each algorithm show relatively high reliability: precision, recall, F1-score and accuracy are greater than 0.84, 0.85, 0.84 and 0.85, respectively. The closer these performance metrics are to 1, the more precise the predicted results.

The mean accuracy for each algorithm is obtained with the stratified k-fold cross-validation technique on the available dataset. A k-fold of 10 is used for the electrotype samples. The MLP algorithm appears to provide the best scoring results for the prediction of electrotypes (Table 4).

4. Discussion

RQI and *FZI* parameters are traditionally calculated from permeability and porosity values and have length units (m). For the target formation, composed considerably of low-permeable rocks, it is ineffective to apply permeability-based *RQI* and *FZI* parameters or calculate permeability by using the core-derived function of porosity.

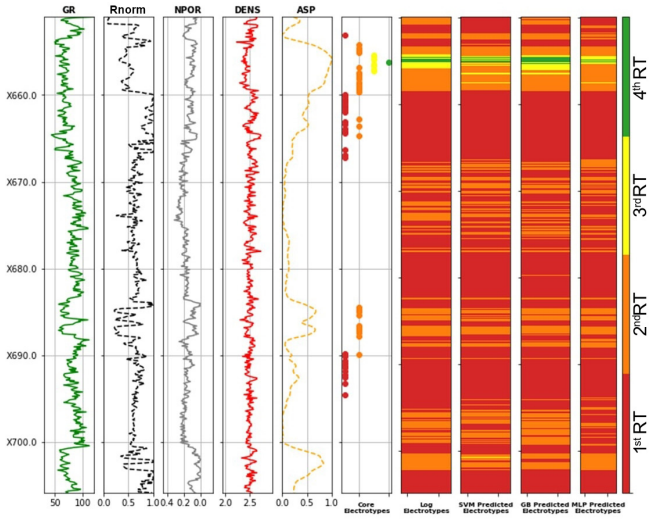

Figure 11. Layout displaying the results of electrotyping by means of ML algorithms: 1st track – measured depth MD (m); 2nd track – gamma ray log (GR) (API); 3nd track – normalized micro-resistivity (v/v); 4th track – neutron log (NPOR) (v/v); 5th track – density log (g/cm³); 6th track – relative spontaneous potential parameter (ASP) (v/v); 7th track – core-derived rock types; 8th – 11th tracks – electrotypes derived from well logs interpretation, SVM prediction, XBG prediction, MLP prediction

As an alternative to common practice, we apply epy dimensionless *FZI* parameter, derived from porosity and irreducible water saturation. This parameter appears to be more effective for low-permeable rocks, wich have much higher variation in S_{wir} rather than in permeability.

A microstructural study supports the rock types derived from the dimensionless *FZI*. Each defined rock type has characteristic parameters of a porous network obtained with CT and NMR tests.

In order to transfer core-derived rock types to well log-derived electrotypes, we apply the same characteristics, namely φ and S_{wir} logs. The integrity of the whole workflow enables very good depth match of the rock types, derived from core and logs.

Since independent well logging data on S_{wir} (for example, from NMR logging) is not available for this project, we calculate S_{wir} log based on k and φ logs, applying corresponding correlation equation, obtained for core data.

To maintain the independence of k and φ in calculating log-derived *FZI*, we calculate permeability not as a function of a porosity log as most practitioners do, but as a function of multiple parameters, namely of V_{clay}, *ASP* and R_{norm}.

We calculate k by applying micro-resistivity log, since it is not affected by fluid type, comparing to deep resistivity logs. We use normalized values of micro-resistivity, in order to mitigate effect of drilling mud conductivity variation in different wells.

Permeability, derived from the multiple logs (R_{norm}, V_{clay} and *ASP*) has the best correlation (R = 0.87) with core-measured permeability, since this set of logs reflects both rock bulk properties as well as porous network characteristics.

Construction of mineralogical model for polymineral rocks requires a sufficient number of logs. Since a sonic log

Algorithm	Well 1		Well 2		Well 3		Well 4		Well 5		Well 6	
	Acc.	F1	Acc.	F1	Acc.	F1	Acc.	F1	Acc.	F1	Acc.	F1
Support Vector Machine	0.86	0.85	0.89	0.89	0.87	0.87	0.83	0.77	0.82	0.80	0.86	0.86
Gradient Boosting Classifier	0.89	0.89	0.91	0.89	0.89	0.89	0.90	0.91	0.73	0.75	0.88	0.88
Multi-Layer Perceptron Classifier	0.85	0.84	0.91	0.91	0.88	0.86	0.94	0.94	0.77	0.75	0.90	0.90

Table 3. Summary of Accuracy (Acc.) and F1-score (F1) after running three ML methods

Algorithm	Model Accuracy Mean
Support Vector Machine	0.852
Gradient Boosting Classifier	0.842
Multi-Layer Perceptron Classifier	0.880

Table 4. Average cross validation score for each ML algorithms based on electrotypes

was not available for all wells, it was reconstructed with ML. Adding the synthesized sonic logs to the data set, applied for calculation of mineralogical content and identification of electrotypes by means of ML, significantly increases reliability of the produced results.

The combination of consistent petrophysical interpretation with supervised machine learning techniques yields geologically minded, reliable and reproducible results. The accuracy of electrotypes prediction by ML amounts to 0.89, thus the selected algorithm, trained even on a relatively limited number of wells, produces reliable results. Therefore, its application can be extended on a larger quantity of wells that will significantly optimize petrophysical interpretation for the whole field.

5. Conclusions

The study developed and successfully applied a new methodology of rock typing and electrotyping of low-resistive, low-permeable clastic reservoirs. The methodology comprises detailed workflow for laboratory tests, rock typing by means of the alternative *FZI* parameter, transfer of core-derived rock types to well log electrotypes, calculation of permeability logs by using a multilinear regression, application of ML for reconstructing lacking logs and extension of electrotypes to uninterpreted wells.

The proposed application of the dimensionless *FZI* parameter, incorporating porosity and irreducible water saturation, proved to be very effective for electrotyping of the formation, including low-resistive and low-permeable intervals.

An effective alternative technique for calculating permeability as a multivariate parameter from independent logs is suggested. The correlation coefficient between measured and predicted permeability amounts to R = 0.87, whereas the R obtained for calculation of k with the traditional method as a function of porosity (φ) is 0.56 only.

The proposed well log interpretation workflow enables conversion of the defined rock types to electrotypes, maintaining the same classification principles for both core and well logs data. This ensures reliable identification of electrotypes in both high and low-permeable rock intervals. Previous studies of this as well as other low-resistive formation could not sufficiently classify the rocks into petrophysically meaningful units.

This study applies supervised ML-assisted electrotyping upon detailed well log interpretation on reference wells that ensures that the results produced are more accurate, consistent, and less prone to bias. Multi-Layer Perceptron algorithm seems to be the most reliable. ML is applied the first time for this low-resistive formation.

Applying the new approaches to rock typing allows detection of productive intervals previously missed and thus enables extending the lifetime of the brownfield.

6. Nomenclature

RCAL – routine core analysis
SCAL – special core analysis
GR – gamma ray log, API
DENSITY – density log, g/cm^3
DT – compressional slowness, μs/m
DT_REC – reconstructed compressional slowness, μs/m
FZI – flow zone indicator, unitless
IR – resistivity index, dimensionless
k – absolute permeability, m^2, mD
M_o – modal pore radius interval, m
M_e – median pore radius interval, m
NMR – nuclear magnetic resonance
NPOR – neutron log, v/v
R_{norm} – normalized resistivity, dimensionless
RT – rock type
RQI – reservoir quality index, unitless
S_w – water saturation volume, %
S_{wir} – irreducible water saturation volume, %
T_2 – relaxation time, s
φ – total porosity, %

Acknowledgments

The authors thank Lukoil Engineering LLC for its financing this research and permission to publish the results of the study. This work was also supported by the Ministry of Science and Higher Education of the Russian Federation under agreement No. 075-15-2020-119 within the framework of the development program for a world-class Research Centre. We thank the Ministry of Science and Higher Education of the Russian Federation for their support. The authors also gratefully acknowledge the Skolkovo Institute of Science and Technology (Russia) for providing a laboratory base for conducting experiments.

Author Contributions

Conceptualization: E. Shvalyuk and A. Tchistiakov.

Methodology: E. Shvalyuk and A. Tchistiakov.

Machine Learning: K. Okosun and E. Shvalyuk.

Petrophysical analysis and interpretation: E. Shvalyuk, A. Tchistiakov, K. Okosun.

Writing – original paper preparation: E. Shvalyuk, A. Tchistiakov, K. Okosun.

Visualization: E. Shvalyuk, K. Okosun.

Scientific supervision and text reviewing: A. Tchistiakov, M. Spasennykh, A. Stenin.

Funding acquisition: A. Tchistiakov, M. Spasennykh, A. Stenin.

References

Abbaszadeh M., Fujii H., Fujimoto F. (1996). Permeability Prediction by Hydraulic Flow Units—Theory and Applications. *SPE Formation Evaluation* 11, pp. 263–271. https://doi.org/10.2118/30158-PA

Akkurt R., Conroy T., Psaila D., Paxton A., Low J. & Spaans P. (2018). Accelerating and enhancing petrophysical analysis with machine learning: A case study of an automated system for well log outlier detection and reconstruction. *SPWLA 59th Annual Logging Symposium 2018*. Society of Petrophysicists and Well-Log Analysts (SPWLA).

Amaefule J.O., Altunbay M., Tiab D., Kersey D.G., and Keelan D.K. (1993). Enhanced reservoir description: using core and log data to identify hydraulic (flow) units and predict permeability in uncored intervals/ wells. *Proceedings - SPE Annual Technical Conference and Exhibition*, pp. 205–220. https://doi.org/10.2523/26436-MS

Archie G.E. (1942). The Electrical Resistivity Log as an Aid in Determining Some Reservoir Characteristics. *Transactions of the AIME,* 146, pp. 54–62. https://doi.org/10.2118/942054-G

Aranibar A., Saneifar M., Heidari Z. (2013). Petrophysical rock typing in organic-rich source rocks using well logs. *Unconventional Resources Technology Conference (URTEC)*. doi: 10.1190/urtec2013-117

Cortes C., Vapnik V. (1995). Support-vector networks. https://doi.org/10.1007/BF00994018

Curtis A.A. (2015). Multi-scale reservoir characterisation from pore scale to simulation scale: Concepts and workflows. *Society of Petroleum Engineers - SPE Reservoir Characterisation and Simulation Conference and Exhibition, RCSC 2015*, pp. 822–842. https://doi:10.2118/175560-ms

Glover P. (2000). Petrophysics MSc Course Notes. Petrophysics MSc Course Notes 32–54.

Gupta, I., Rai, C., Sondergeld, C., Devegowda, D. (2018). Rock Typing in Eagle Ford, Barnett, and Woodford Formations. *SPE Reservoir Evaluation & Engineering*, 21, pp. 654–670. https://doi.org/10.2118/189968-PA

Eltom H.A. (2020). Limitation of laboratory measurements in evaluating rock properties of bioturbated strata: A case study of the Upper Jubaila Member in central Saudi Arabia. *Sedimentary Geology,* 398, 105573. https://doi.org/10.1016/j.sedgeo.2019.105573

Gholami V., Mohaghegh S.D. (2009). Intelligent Upscaling of Static and Dynamic Reservoir Properties. *Presented at the SPE Annual Technical Conference and Exhibition,* New Orleans, Louisiana, SPE-124477-MS. https://doi.org/10.2118/124477-MS

Guo G., Diaz M.A., Paz F., Smalley J., Waninger E.A. (2007). Rock Typing as an Effective Tool for Permeability and Water-Saturation Modeling: A Case Study in a Clastic Reservoir in the Oriente Basin. *SPE Reservoir Evaluation & Engineering*, 10, pp. 730–739. https://doi.org/10.2118/97033-PA

Kassem A., Hemdan K., Saad A. (2017). Integration of petrology and petrophysical rock typing for optimum reservoir zonation and permeability prediction (Case study: North gulf of Suez. Egypt). *Offshore Mediterranean Conference and Exhibition*, OMC 2017.

Kolodzie S. (1980). Analysis of pore throat size and use of the Waxman - Smits equation to determine OOIP in spindle field, Colorado. *Proceedings - SPE Annual Technical Conference and Exhibition.* Society of Petroleum Engineers (SPE). doi: 10.2118/9382-ms

Kotsiantis S. B. (2007). Supervised Machine Learning: A Review of Classification Techniques. *Informatica,* 31, pp. 249–268.

Ma D., Liu, C., Cheng C. (2015). New relationship between resistivity index and relative permeability. *Journal of Energy Resources Technology, Transactions of the ASME*, 137. doi:10.1115/1.4028862

Man, H.Q., Jarzyna, J. (2013). Integration of core, well logging and 2D seismic data to improve a reservoir rock model: a case study of gas accumulation in the NE Polish Carpathian Foredeep. GQ 57. https://doi.org/10.7306/gq.1091

Man H.Q., et al., (2021). Hydraulic Flow Unit Classification and Prediction Using Machine Learning Techniques: A Case Study from the Nam Con Son Basin, Offshore Vietnam. *Energies,* 14, 7714. https://doi.org/10.3390/en14227714

Merembayev T., Kurmangaliyev D., Bekbauov B., Amanbek Y.A. (2021). Comparison of Machine Learning Algorithms in Predicting Lithofacies: Case Studies from Norway and Kazakhstan. *Energies*, 14, 1896. https://doi.org/10.3390/en14071896

Mustafa A., Mahmoud A.M., Abdulraheem A. (2019). A Review of Pore Structure Characterization of Unconventional Tight Reservoirs, in: Day 3 Wed, November 13, 2019. *Presented at the Abu Dhabi International Petroleum Exhibition & Conference,* Abu Dhabi, UAE, D031S098R001. https://doi.org/10.2118/197825-MS

Nelson, P.H. (1994). Permeability-porosity relationships in sedimentary rocks. *Log Analyst,* 35, pp. 38–62.

Onovughe E., Sofolabo A. (2016). Saturation Modelling: Using the Waxman - Smits Model/Equation In Saturation Determination In Dispersed Shaly Sands. Journal of Multidisciplinary Engineering Science and Technology, 3(6).

Perez H.H., Datta-Gupta A., Mishra S. (2005). The Role of Electrofacies, Lithofacies, and Hydraulic Flow Units in Permeability Prediction From Well Logs: A Comparative Analysis Using Classification Trees. *SPE Reservoir Evaluation & Engineering,* 8, pp. 143–155. https://doi.org/10.2118/84301-PA

Perry S.E., Hayes D. (2019). Presenting a multifaceted approach to unconventional rock typing and technical validation-case study in the Permian basin and impacts on reservoir characterization workflows. *Petrophysics,* 60, pp. 641–659. doi: 10.30632/pjv60n5-2019a8

Pirson S.J., Boatman E.M., Nettle R.L. (1963). Prediction of relative permeability characteristics of intergranular reservoir rocks from electrical resistivity measurements. *SPWLA 4th Annual Logging Symposium*. Society of Petrophysicists and Well-Log Analysts (SPWLA). https://doi:10.2118/749-pa

Pittman E.D. (1992). Relationship of porosity and permeability to various parameters derived from mercury injection-capillary pressure curves for sandstone. *American Association of Petroleum Geologists Bulletin,* 76, pp. 191–198. doi:10.1306/bdff87a4-1718-11d7-8645000102c1865d

Sarkar D., Bali R., Sharma T. (2018). Practical Machine Learning with Python: A Problem-Solver's Guide to Building Real-World Intelligent Systems. https://doi.org/10.1007/978-1-4842-3207-1

Saxena, N., et al., (2019). Rock properties from micro-CT images: Digital rock transforms for resolution, pore volume, and field of view. *Advances in Water Resources,* 134, 103419. https://doi.org/10.1016/j.advwatres.2019.103419

Smits, L.J.M. (1968). SP Log Interpretation in Shaly Sands. *Society of Petroleum Engineers Journal,* 8, pp. 123–136. https://doi.org/10.2118/1863-B

Shvalyuk, E., Tchistiakov, A., Kalugin, A. (2021). The Application of Computed Tomography Scanning and Nuclear Magnetic Resonance for Rock Typing of Polymineral Clastic Reservoirs. *SPE Reservoir Evaluation & Engineering,* SPE-208603-PA. https://doi.org/10.2118/208603-PA

Teh W.J., Willhite G.P., Doveton J.H. (2012). Improved Reservoir Characterization using Petrophysical Classifiers within Electrofacies. In: All Days. *Presented at the SPE Improved Oil Recovery Symposium,* Tulsa, Oklahoma, USA, SPE-154341-MS. https://doi.org/10.2118/154341-MS

Tiab D., Donaldson E.C. (2016). Petrophysics (Fourth Edition). Elsevier Inc. https://doi.org/10.1016/C2014-0-03707-0

Vernik L. (2000). Permeability prediction in poorly consolidated siliciclastics based on porosity and clay volume logs. *Log Analyst,* 41, pp. 138–147.

Wang X., Wang J., Guan Let al., (2023). Intelligent Wireline Formation Tester Evaluation of Low-Permeability and Low-Resistivity-Contrast Formation. *Presented at the Offshore Technology Conference*, D041S045R007. https://doi.org/10.4043/32269-MS

Waxman M.H., Smits L.J.M. (1968). Electrical Conductivities in Oil-Bearing Shaly Sands. *Society of Petroleum Engineers Journal,* 8, pp. 107–122. https://doi.org/10.2118/1863-A

About the Authors

Alexei Tchistiakov – Associate Professor, Center for Petroleum Science and Engineering, Skolkovo Institute of Science and Technology

Buil. 1, 30, Bolshoy Boulevard, Moscow, 121205, Russian Federation

e-mail: A.Tchistiakov@skoltech.ru

Elizaveta Shvalyuk – PhD student, Center for Petroleum Science and Engineering, Skolkovo Institute of Science and Technology
Buil. 1, 30, Bolshoy Boulevard, Moscow, 121205, Russian Federation
e-mail: elizaveta.shvalyuk@skoltech.ru

Kenneth Okosun – MSc student, Center for Petroleum Science and Engineering, Skolkovo Institute of Science and Technology
Buil. 1, 30, Bolshoy Boulevard, Moscow, 121205, Russian Federation

Mikhail Spasennykh – Professor, Director of the Center for Petroleum Science and Engineering, Skolkovo Institute of Science and Technology
Buil. 1, 30, Bolshoy Boulevard, Moscow, 121205, Russian Federation
e-mail: m.spasennykh@skoltech.ru

Alexei Stenin – Head of the Department, LUKOIL-Engineering LLC
Build. 1, 3, Pokrovsky Boulevard, Moscow, 109028, Russian Federation

Manuscript received 5 June 2024;
Accepted 27 September 2024; Published 20 December 2024

IN RUSSIAN

ОРИГИНАЛЬНАЯ СТАТЬЯ

Новая методика интерпретации данных ГИС для надежной петротипизации низкопроницаемых и низкоомных коллекторов

А. Чистяков[1], Е. Швалюк[1], К. Окосун[1], М. Спасенных[1], А. Стенин[2]*
[1]Сколковский институт науки и технологий, Москва, Россия
[2]ООО «ЛУКОЙЛ-Инжиниринг», Москва, Россия
Ответственный автор: Алексей Чистяков, e-mail: sharafv@inbox.ru

Аннотация. Целевой пласт месторождения нефти, расположенного в Западной Сибири, слагается терригенными породами, представленными в основании алевролитами, плавно переходящими в песчаники вверх по разрезу. Из-за отсутствия детальной петротипизации алевролиты, имеющие более низкие значения электрического сопротивления и проницаемости, были первоначально отнесены к водоносной части разреза. Однако последующие испытания скважин выявили в них значительный приток нефти.

Для проведения корректного расчета насыщенности и выделения нефтеносных интервалов в низкоомных терригенных коллекторах в рамках данного исследования была разработана новая методика их типизации. Методика включает в себя детальное описание программы лабораторных исследований, процедуру типизации пород с применением альтернативного индикатора зоны потока (FZI), а также алгоритм выделения в разрезах скважин по данным ГИС петрофизических типов, соответствующих выделенным по керну типов пород (роктипов).

Применение предложенного безразмерного параметра FZI, включающего пористость и остаточную водонасыщенность, оказалось весьма эффективным для петротипизации пласта, включая низкоомные и низкопроницаемые интервалы. При этом следует особо подчеркнуть, что разработанный алгоритм интерпретации данных каротажа позволяет транслировать выделяемые по керну типы пород в выделяемые по данным ГИС петрофизические типы, сохраняя одинаковые критерии классификации.

Так как низкопроницаемые интервалы характеризуются низкой корреляцией между проницаемостью и пористостью, использование параметра пористости, определённого методами ГИС для расчета профиля проницаемости, приводит к ненадежному результату. Для решения этой проблемы в работе реализуется альтернативная методика расчета проницаемости на основании множественной корреляции с данными нескольких методов ГИС.

Для оптимизации практической реализации новых методик предлагается несколько алгоритмов машинного обучения, позволяющих реконструировать отсутствующие каротажные кривые, а также распространять выделенные петротипы на разрезы скважин, в которых детальная петрофизическая интерпретация еще не проводилась.

Разработанные подходы к петротипизации низкоомных и низкопроницаемых пород позволяют обнаруживать ранее пропущенные продуктивные интервалы, что продлит срок экономической рентабельности изученных месторождений.

Ключевые слова: ГИС, роктипизация, низкоомные, низкопроницаемые коллекторы, петротипизация, машинное обучение

Для цитирования: Thistiakov A., Shvalyuk E., Okosun K., Spasennykh M., Stenin A. (2024). Advanced Well Logging Interpretation for Reliable Electrotyping of Low-permeable and Low-resistivity Formation. *Georesursy = Georesources*, 26(4), pp. 163–175. https://doi.org/10.18599/grs.2024.4.20

Финансирование/Благодарности

Авторы благодарят ООО «Лукойл Инжиниринг» за финансирование исследования и разрешение на публикацию его результатов. Работа поддержана Министерством науки и высшего образования Российской Федерации по договору № 075-15-2020-119 в рамках программы развития Научного центра мирового уровня. Мы благодарим Министерство науки и высшего образования Российской Федерации за поддержку. Авторы выражают благодарность Сколковскому институту науки и технологий за предоставление лабораторной базы для проведения экспериментов.

Сведения об авторах

Алексей Чистяков – доцент, Центр науки и технологий добычи углеводородов, Сколковский институт науки и технологий

Россия, 121205, Москва, Большой бульвар, д. 30, стр.1

e-mail: A.Tchistiakov@skoltech.ru

Елизавета Швалюк – аспирант, Центр науки и технологий добычи углеводородов, Сколковский институт науки и технологий

Россия, 121205, Москва, Большой бульвар, д. 30, стр.1

e-mail: elizaveta.shvalyuk@skoltech.ru

Кеннет Окосун – студент магистратуры, Центр науки и технологий добычи углеводородов, Сколковский институт науки и технологий

Россия, 121205, Москва, Большой бульвар, д. 30, стр.1

Михаил Спасенных – кандидат хим. наук, профессор, директор Центра науки и технологий добычи углеводородов, Сколковский институт науки и технологий

Россия, 121205, Москва, Большой бульвар, д. 30, стр.1

e-mail: m.spasennykh@skoltech.ru

Алексей Стенин – руководитель отдела

ООО «ЛУКОЙЛ-Инжиниринг»

Россия, 109028, Москва, Покровский бульвар, д. 3, стр. 1

Статья поступила в редакцию 5.06.2024;
Принята к публикации 27.09.2024; Опубликована 20.12.2024